**Revision 1**

# Maruyamaite, $K(MgAl_2)(Al_5Mg)Si_6O_{18}(BO_3)_3(OH)_3O$, a potassium-dominant tourmaline from the ultrahigh-pressure Kokchetav massif, northern Kazakhstan: Description and crystal structure

Aaron Lussier[1,2], Neil A. Ball[1], Frank C. Hawthorne[1,*], Darrell J. Henry[3], Rentaro Shimizu[4], Yoshihide Ogasawara[4] and Tsutomu Ota[5]

[1] Department of Geological Sciences, University of Manitoba Winnipeg, MB, R3T 2N2, Canada

[2] Current address: Department of Civil and Environmental Engineering and Earth Sciences, University of Notre Dame, Notre Dame, IN 46556, USA

[3] Department of Geology and Geophysics, Louisiana State University, Baton Rouge, LA 70803, USA

[4] Department of Earth Sciences, Waseda University, 1-6-1 Nishiwaseda, Shinjuku-ku, Tokyo 169-8050, Japan

[5] Pheasant Memorial Laboratory for Geochemistry and Cosmochemistry, Institute for the Study of the Earth's Interior, Okayama University, Misasa, Tottori, 682-0193, Japan

* E-mail: frank_hawthorne@umanitoba.ca

## ABSTRACT

Maruyamaite, ideally $K(MgAl_2)(Al_5Mg)Si_6O_{18}(BO_3)_3(OH)_3O$, was recently approved as the first K-dominant mineral-species of the tourmaline supergroup. It occurs in ultra-high pressure quartzofeldspathic gneisses of the Kumdy-Kol area of the Kokchetav Massif, northern Kazakhstan. Maruyamaite contains inclusions of microdiamonds, and probably crystallized near the peak pressure conditions of UHP metamorphism in the stability field of diamond. Crystals occur as anhedral to euhedral grains up to 2 mm across, embedded in a matrix of anhedral quartz and K-feldspar. Maruyamaite is pale brown to brown with a white to very pale-brown streak and has a vitreous luster. It is brittle and has a Mohs hardness of ~7; it is non-fluorescent, has no observable cleavage or parting, and has a calculated density of 3.081 $gcm^{-3}$. In plane-polarized transmitted light, it is pleochroic, O = darkish brown, E = pale brown. Maruyamaite is uniaxial negative, $\omega = 1.634$, $\varepsilon = 1.652$, both ±0.002. It is rhombohedral, space group *R*3*m*, $a = 15.955(1)$, $c = 7.227(1)$ Å, $V = 1593(3)$ $Å^3$, $Z = 3$. The strongest ten X-ray diffraction lines in the powder pattern are [d in Å(I)(hkl)]: {note to typesetting: minus signs are overbars on top of the following digit} 2.581(100)(051), 2.974(85)(-132), 3.995 (69)(-240), 4.237(59)(-231), 2.046(54)(-162), 3.498(42)(012), 1.923(36)(-372), 6.415(23)(-111), 1.595(22)(-5.10.0), 5.002(21)(021) and 4.610(20)(030). The crystal structure of maruyamaite was refined to an $R_1$ index of 1.58% using 1149 unique reflections measured with Mo*K*a X-radiation. Analysis by a combination of electron microprobe and crystal-structure refinement gave $SiO_2$ 36.37, $Al_2O_3$ 31.50, $TiO_2$ 1.09, $Cr_2O_3$ 0.04, $Fe_2O_3$ 0.33, FeO 4.01, MgO 9.00, CaO 1.47, $Na_2O$ 0.60, $K_2O$ 2.54, F 0.30, $B_2O_3$(calc) 10.58, $H_2O$(calc) 2.96, sum 100.67 wt%. The formula unit, calculated on the basis of 31 anions pfu with B = 3, OH = 3.24 apfu (derived from the crystal structure) and the site populations

assigned to reflect the mean interatomic distances, is $(K_{0.53}Na_{0.19}Ca_{0.26}\square_{0.02})_{\Sigma X=1.00}$ $(Mg_{1.19}Fe^{2+}_{0.55}Fe^{3+}_{0.05}Ti_{0.14}Al_{1.07})_{\Sigma Y=3.00}(Al_{5.00}Mg_{1.00})(Si_{5.97}Al_{0.03}O_{18})(BO_3)_3(OH)_3(O^{2-}_{0.60}$ $F_{0.16}OH_{0.24})$. Maruyamaite, ideally $K(MgAl_2)(Al_5Mg)(BO_3)_3(Si_6O_{18})(OH)_3O$, is related to oxydravite: ideally $Na(MgAl_2)(Al_5Mg)(BO_3)_3(Si_6O_{18})(OH)_3O$, by the substitution $^{X}K \rightarrow {}^{X}Na$.

*Keywords:* Maruyamaite, tourmaline, new mineral, electron-microprobe analysis, optical properties, crystal-structure refinement, Kokchetav Massif, northern Kazakhstan, ultrahigh-pressure, microdiamond inclusions.

## INTRODUCTION

The general formula of the minerals of the tourmaline supergroup can be written as

$$X\,Y_3\,Z_6\,[T_6O_{18}]\,[BO_3]_3\,V_3\,W$$

where $X$ = Na, K, Ca, $Pb^{2+}$, Bi, □ (vacancy); $Y$ = Li, Mg, $Fe^{2+}$, $Mn^{2+}$, Al, $Cr^{3+}$, $V^{3+}$, $Fe^{3+}$, $Ti^{4+}$; $Z$ = Mg, $Fe^{2+}$, Al, $Fe^{3+}$, $V^{3+}$, $Cr^{3+}$; $T$ = Si, Al, B; $B$ = B; $V$ = OH, O; $W$ = OH, F, O. The tourmaline supergroup minerals are important indicator minerals, providing both chemical (e.g., Selway et al. 1998a,b, 1999, 2000a, b, 2002; Novák et al. 2004, 2011; Agrosì et al. 2006; Lussier and Hawthorne 2011; Lussier et al. 2008, 2011a,b; Hawthorne and Dirlam 2011; Henry and Dutrow 1990, 1996; Dutrow and Henry 2011; Bačík et al. 2011; van Hinsberg and Schumacher 2009; van Hinsberg et al. 2011a) and isotopic (e.g., Marschall et al. 2006; van Hinsberg and Marschall 2007; Ludwig et al. 2011; Marschall and Jiang 2011; van Hinsberg et al. 2011b; Shabaga et al. 2010; Hezel et al. 2011) information on the evolution of their host rocks. However, the chemical composition of tourmalines is also controlled by short-range and long-range constraints (e.g., Hawthorne 1996, 2002; Hawthorne and Henry 1999; Bosi and Lucchesi 2007; Bosi 2010, 2011, 2013; Bosi et al. 2010; Henry and Dutrow 2011; Skogby et al. 2012). The dominant constituents at the X site are Na, Ca and □, and until now, the remaining constituents, K, $Pb^{2+}$ and Bi, have been found only in subordinate amounts. However, Ota et al. (2008a,b) and Shimizu and Ogasawara (2013) reported K-rich and K-dominant tourmaline from diamondiferous Kokchetav UHP metamorphic rocks in northern Kazakhstan (Kaneko et al. 2000). Here we describe a new $^{X}$K-dominant tourmaline from these rocks. The new species and name have been approved by the International Mineralogical Association Commission on New Minerals, Nomenclature and Classification (2013-123). Maruyamaite is named in honour of Professor Shigenori Maruyama (Earth-Life Science Institute, Tokyo Institute of Technology, Japan), born 24th December, 1949,

in Tokushima, Japan. Professor Maruyama is a prominent figure in the field of regional tectonics and led the project which unraveled the mechanism of continental subduction and exhumation (from a depth greater than 120 km) of the Kokchetav massif of northern Kazakhstan, and discovered the diamond-bearing UHP rocks that contain the new K-dominant tourmaline. Holotype material is deposited in the collections of the National Museum of Nature and Science, Tsukuba, Japan, registered number NSM- MF15696.

## OCCURRENCE

Maruyamaite occurs as core domains of chemically zoned tourmaline in a quartzofeldspathic rock collected from the Kumdy-Kol area of the Kokchetav Massif (Ota et al. 2008a,b; Shimizu and Ogasawara 2013). The rock occurs as thin layers of variable thickness (less than several cm) in diamond-bearing pelitic gneiss, and consists mainly of quartz, K-feldspar and tourmaline (up to 20 vol%) with minor amounts of goethite, titanite, zircon, phengite, phlogopite, apatite, chlorite, zoisite, pumpellyite, graphite and diamond. Tourmaline occurs as anhedral to euhedral crystals up to 2 mm across with strong chemical zoning; K decreases from core to rim (Fig. 1). Although the mantle and rim also contain high amounts of K for magnesian tourmaline, their K-contents in atoms per formula unit (apfu) do not exceed those of Na or Ca (i.e., the mantle and the rim compositions correspond to K-bearing dravite or oxy-dravite). Microdiamond inclusions occur only in the K-dominant core of tourmaline (maruyamaite) and in zircon. On the other hand, flake graphite and quartz occur in the mantle and rim. More detailed descriptions of the chemical zoning and inclusion content of tourmaline in these rocks are given by Shimizu and Ogasawara (2013).

## PHYSICAL PROPERTIES

Maruyamaite is pale brown to brown with a white to very pale-brown streak, has a vitreous luster and does not fluoresce in ultraviolet light. It has a Mohs hardness of ~7, and is brittle with a splintery fracture; the calculated density is 3.081 g $cm^{-3}$. A spindle stage was used to orient a crystal for measurement of optical properties. The optical orientation was determined by transferring the crystal from the spindle stage to a single-crystal diffractometer and measuring the relative axial relations by X-ray diffraction. In transmitted polarized light, maruyamaite is pleochroic with O = darkish brown, E = pale brown. It is uniaxial negative, with indices of refraction $\omega = 1.634$, $\varepsilon = 1.652$, both ±0.002, measured with gel-filtered Na light ($\lambda = 589.9$ nm).

## RAMAN SPECTROSCOPY

Raman spectra of maruyamaite were obtained using an $Ar^{+}$ laser with a wavelength of 514.5nm. The Raman spectra (Fig. 2) show a strong single band at 3572 $cm^{-1}$. The peak may be assigned to an O-H stretching band involving (OH) at the O3 site. Below 1500 $cm^{-1}$, there is a very weak band at 1230 $cm^{-1}$ (internal modes of the $BO_3$ group), a group of bands (977 m, 1051 m, 1106 sh) centered on ~1000 $cm^{-1}$ (internal modes of the $SiO_4$ group), another group of bands (669 m, 703 s, 789 vs) centered on ~720 $cm^{-1}$ (delocalised $Si_6O_{18}$ ring motions and $AlO_6$ deformations), and lower-frequency bands at 538 vw, 500 w, 367 vs, 242 m, 212 s and 155 w $cm^{-1}$ (vs = very strong, s = strong, m = medium, w = weak, vw = very weak, sh = shoulder) (various motions involving the more weakly bonded cations K, Na, Mg). Assignments follow those of McKeown (2008).

## MÖSSBAUER SPECTROSCOPY

The Mössbauer spectrum was collected in transmission geometry at room temperature (RT) using a $^{57}$Co point source. The spectrometer was calibrated using the RT spectrum of α-Fe. For preparing the Mössbauer absorber, several K-tourmaline grains were attached to adhesive tape and mounted on a Pb disk with a 500 μm aperture, and the collection time was one month. The spectrum was analyzed using a Voigt-based quadrupole-splitting distribution (QSD) method (Rancourt and Ping 1991). To account for thickness and/or instrumental broadening, the Lorentzian linewidth of the symmetrical elemental doublets of the QSD was allowed to vary during spectrum fitting. There are two symmetrical doublets with Mössbauer parameters typical of octahedrally coordinated $Fe^{2+}$ and one doublet with parameters typical of octahedrally coordinated $Fe^{3+}$ (Fig. 3, Table 1). The area ratio of the $Fe^{3+}$ doublet to the $Fe^{2+}$ doublets is 0.076 : 0.924, and this value was also taken as the $Fe^{3+}$ : $Fe^{2+}$ ratio (i.e., assuming equal recoil-free fractions for $Fe^{2+}$ and $Fe^{3+}$).

## CHEMICAL COMPOSITION

The crystal used for the collection of the X-ray intensity data was embedded in epoxy, polished, carbon coated and analyzed with a Cameca SX-100 electron microprobe operating in wavelength-dispersion mode with an excitation voltage of 15 kV, a specimen current of 10 nA, a beam diameter of 10 μm, peak count-times of 20 s and background count-times of 10 s. The following standards and crystals were used: Si, Mg, Ca: diopside, TAP, LTAP,LPET; Ti: magnesio-hornblende, LLiF; Fe: fayalite, LLiF; Mn: rhodonite, LLiF; Na: albite, TAP; Al: andalusite, TAP; K: orthoclase, LPET; F: fluoro-riebeckite, LTAP; Zn: willemite, LLiF; Cr: chromite, LLiF. Data reduction was done using the φ(ρZ) procedure of Pouchou and Pichoir

(1985). The average of eleven analyses on a single grain is given in Table 2.

## X-RAY POWDER DIFFRACTION

X-ray powder-diffraction data were collected with a Bruker D8 Discover SuperSpeed micro-powder diffractometer with a multi-wire 2D detector using a modified Gandolfi attachment (Cu*K*α, λ = 1.54178 Å); 50kV/60 mA; two 30 min. frames, merged; no internal standard used. Data were indexed on the following refined cell-dimensions: $a$ = 15.915(3), $c$ = 7.120(2) Å, V = 1561.8(7) Å$^3$, and the pattern is given in Table 3.

## CRYSTAL-STRUCTURE REFINEMENT

A fragment was extracted from the center of a strongly zoned crystal of maruyamaite in thin section, attached to a tapered glass fiber and mounted on a Bruker APEX II ULTRA three-circle diffractometer equipped with a rotating-anode generator (Mo*K*a), multilayer optics and an APEX II 4K CCD detector. A total of 6230 intensities was collected to 60º2θ using 2 s per 0.2º frame and a crystal-to-detector distance of 5 cm. Empirical absorption corrections (SADABS; Sheldrick 2008) were applied and equivalent reflections were corrected for Lorentz, polarization and background effects, averaged and reduced to structure factors. The unit-cell dimensions were obtained by least-squares refinement of the positions of 4678 reflections with $I > 10\sigma I$ and are given in Table 4, together with other information pertaining to data collection and structure refinement.

All calculations were done with the SHELXTL PC (Plus) system of programs. The structure was refined by full-matrix least-squares methods with anisotropic-displacement parameters for all atoms, and converged to a final R1 index of 1.58%. Refined atom coordinates

and anisotropic-displacement parameters are listed in Table 5, selected interatomic distances are given in Table 6, and refined site-scattering values (Hawthorne et al. 1995) and assigned site-populations are given in Table 7. The CIF is on deposit and available as listed below.[1]

## CHEMICAL FORMULA

In the absence of a determination of $H_2O$ content, the chemical composition (Table 2) of tourmaline was initially reduced to a chemical formula on the basis of 31 anions per formula unit with B = 3 apfu and (OH) + F = 4 apfu, and the resulting formula provided a starting point for a more accurate normalization. For maruyamaite, the Y- and Z-site contents, together with the observed <Y-O> and <Z-O> distances (Table 6), indicate that there is significant disorder of Mg and Al over the Y and Z sites. Taylor et al. (1995) refined the structure of an OH-deficient uvite with significant disorder of this type, and Hawthorne (1996) has discussed how the bond-valence requirements for O at the O1 site can drive the order-disorder reaction $^{Y}Al + {}^{Z}Mg = {}^{Y}Mg + {}^{Z}Al$. This issue has been examined in more detail by Bosi (2013) who produced the expression $^{O1}(OH) = 2 - 1.01\Sigma s^{O(1)} - 0.21 - F$ apfu to estimate the amount of (OH) at the O1 site where $\Sigma s^{O(1)}$ is the bond valence incident at the O1 anion (exclusive of H). We used this expression to estimate the amount of (OH) at O1 and then renormalized the chemical formula on this basis. We again recalculated the $^{O1}(OH)$ content on the basis of the new formula, and iterated this process to convergence. There is the possibility of $^{X}K$ bonding to O1, but the observed distance of 3.218 Å results in an additional 0.03 v.u. incident at O1 and a negligible change (0.02 apfu) in the (OH) content. The final calculated (OH) content of the crystal is 3.24 apfu, and calculation of the

[1] Deposit item AM-XX-XXX, CIF, is stored on the MSA web site and available via the American Mineralogist Table of Contents. Find the article in the table of contents at GSW (ammin.geoscienceworld.org) or MSA (www.minsocam.org), and then click on the deposit link.

empirical chemical formula with this OH content gave the following result:

$(K_{0.53}Na_{0.19}Ca_{0.26}\square_{0.02})_{\Sigma X=1.00}(Mg_{2.20}Fe^{2+}_{0.55}Fe^{3+}_{0.05}Ti_{0.14}Al_{0.07})_{\Sigma Y=3.01}(Al_6)(Si_{5.97}Al_{0.03}O_{18})$ $(BO_3)_3(OH)_3(O^{2-}_{0.60}F_{0.16}OH_{0.24})$.

## SITE POPULATIONS

The T site is almost completely occupied by Si according to the formula derived from the electron-microprobe analysis, and the <T-O> distance (Table 6) is 1.621 Å, close to the value of 1.620 Å proposed as the <Si-O> distance in the tourmaline structure by MacDonald and Hawthorne (1995). Although the Z site in the tourmaline structure is dominated by Al, Hawthorne et al. (1993) showed that there is significant disorder of Al and Mg over the Y and Z sites in tourmaline, and the <Z-O> distance is sensitive to occupancy by other cations (Hawthorne et al. 1993; Burns et al. 1994; Bosi 2008, 2011; Bosi and Lucchesi 2004; Bosi and Skoby 2013; Bosi et al. 2004; Clark et al. 2011; Ertl et al. 2010a,b; Novák et al. 2013). Where Z is completely occupied by Al, the <Z-O> distances are in the range 1.904-1.910 Å (e.g., Hawthorne et al. 1993; Bosi 2008; Lussier et al. 2011a; MacDonald et al. 1993; Selway et al. 1998a,b). Bosi and Lucchesi (2007) showed that <Z-O> distances are also inductively affected by different occupancies at the Y site. The <Z-O> distance varies linearly with the mean radius of the constituent Z cations, and the <Z-O> distance in the holotype maruyamaite structure (1.932 Å, Table 6) is significantly longer than the values for tourmaline structures where Z = $Al_6$ (1.904-1.911 Å, see above), indicating that maruyamaite has significant disorder of Mg and Al over the Y- and Z-sites, as discussed above. In Figure 4, the <Z-O> distance in maruyamaite (1.932 Å) intersects the line through the rest of the data at 5.00 Al pfu (marked by the pink diamond in Fig. 4), and hence the site population of Z was set at $Al_{5.00}Mg_{1.00}$ apfu and the site

214 population of Y was modified accordingly.

215 The resultant site-populations for maruyamaite are given in Table 7. Maruyamaite,
216 ideally $K(MgAl_2)(Al_5Mg)(BO_3)_3(Si_6O_{18})(OH)_3O$, is the K analogue of oxy-dravite, ideally
217 $Na(MgAl_2)(Al_5Mg)(BO_3)_3(Si_6O_{18})(OH)_3O$ (Bosi and Skogby 2013), and the new rootname is in
218 accord with Henry et al. (2011), the current IMA-approved nomenclature for the tourmaline
219 supergroup minerals.

220

221 **DISCUSSION**

222 The direct association of maruyamaite with diamond inclusions at the Kokchetav locality
223 suggests that high K contents in magnesian tourmaline may be an indicator of UHP conditions.
224 However, tourmaline developed in other UHP terrains typically do not exhibit comparable K
225 contents, and generally contain <0.05 apfu K (cf. Ertl et al. 2010b). This apparent inconsistency
226 was examined in the experimental study of Berryman et al. (2014) who found that K contents in
227 synthetic dravitic tourmalines in K-bearing aqueous fluids increase to K-dominant contents at
228 UHP conditions. However, with significant amounts of Na and K in the aqueous fluids, the
229 amount of K in the synthetic tourmaline was greatly reduced under UHP conditions.

230 Significant amounts of K occur in povondraite (Grice et al. 1993; Zácek et al. 2000), a
231 tourmaline in which $Fe^{3+}$ dominates over Al and which forms at relatively low pressure,
232 suggesting that tourmalines with high contents of $Fe^{3+}$ can accommodate far more K than Al-rich
233 tourmaline at low pressure. The implication is that K-dominant magnesian tourmalines such as
234 maruyamaite are not only a function of UHP conditions, but also the presence of highly potassic
235 fluids.

236

## IMPLICATIONS

The crystallization of maruyamaite requires both UHP conditions and K-dominated compositions, and these conditions could occur by partial melting of subducted continental crust (including sedimentary rocks) at high pressure in the stability field of diamond (Ota et al. 2008a,b). This conclusion is consistent with previous studies (e.g., Hwang et al. 2005) which have shown that K-rich fluid was present at the Kokchetav UHP stages and played an important role in the formation of metamorphic diamond and other UHP minerals such as K-rich clinopyroxene.

As neither maruyamaite nor other tourmalines have been found in diamond-bearing zircon (Shimizu and Ogasawara 2013), and both K-tourmaline and dravite are likely to be unstable at peak metamorphic conditions of the Kokchetav Massif (> 6Gpa, e.g., Ogasawara et al. 2002) according to Ota et al. (2008a,b) and Berryman et al. (2014), it is probable that maruyamaite formed during exhumation after peak metamorphism (but still at UHP conditions). The discovery of maruyamaite and related K-rich tourmaline in the Kokchetav UHP rocks highlights the potential of tourmaline as a recorder of metamorphic history.

Wunder et al. (2015) showed that tourmaline can incorporate small amount of nitrogen as $NH_4^+$ (which has an ionic radius similar to that of K) at high pressure. High-pressure tourmalines, including maruyamaite, can be a container of volatile elements such as H, B and N in the deep mantle, and play an important role in the recycling of crustal material.

## ACKNOWLEDGEMENTS

We thank Andreas Ertl and an anonymous reviewer for their useful comments on this paper. This work was supported by a University of Manitoba Graduate Fellowship to AL, a

Canada Research Chair in Crystallography and Mineralogy to FCH, and by Natural Sciences and Engineering Research Council of Canada Discovery, Research Tools and Equipment, and Major Facilities Access grants, and by Canada Foundation for Innovation grants, to FCH. Some investigations of the petrologic applications of tourmaline benefited from NSF funding to DJH from grant EAR-9405747. The petrographic work and Raman spectroscopy were funded by the Japan Society for the Promotion of Science Grant-in-Aid no. 15204050 to YO.

## REFERENCES

Agrosì, G., Bosi, F., Lucchesi, S., Melchiorre, G., and Scandale, E. (2006) Mn-tourmaline crystals from island of Elba (Italy): Growth history and growth marks. American Mineralogist, 91, 944–952.

Bačík, P., Méres Š., and Uher, P. (2011) Vanadium-bearing tourmaline in metacherts from Chvojnica, Slovak Republic: crystal chemistry and multistage evolution. Canadian Mineralogist, 49, 195–206.

Berryman, E., Wunder, B., and Rhede, D. (2014) Synthesis of K-dominant tourmaline. American Mineralogist, 99, 539–542.

Bosi, F. (2008) Disordering of $Fe^{2+}$ over octahedrally coordinated sites of tourmaline. American Mineralogist, 93, 1647–1653.

——— (2010) Octahedrally coordinated vacancies in tourmaline: a theoretical approach. Mineralogical Magazine, 74, 1037–1044.

——— (2011) Stereochemical constraints in tourmaline: from a short-range to a long-range structure. Canadian Mineralogist, 49, 17–27.

——— (2013) Bond-valence constraints around the O1 site of tourmaline. Mineralogical Magazine, 77, 343–351.

Bosi, F., and Lucchesi, S. (2004) Crystal chemistry of the schorl-dravite series. European Journal of Mineralogy, 16, 335–344.

——— (2007) Crystal chemical relationships in the tourmaline group: Structural constraints on chemical variability. American Mineralogist, 92, 1054–1063.

Bosi, F., and Skogby, H. (2013) Oxy-dravite, $Na(Al_2Mg)(Al_5Mg)(Si_6O_{18})(BO_3)_3(OH)_3O$, a new mineral species of the tourmaline supergroup. American Mineralogist, 98, 1442–1448.

Bosi, F., Lucchesi, S., and Reznitskii, L. (2004) Crystal chemistry of the dravite-chromdravite series. European Journal of Mineralogy, 16, 345–352.

Bosi, F., Balić-Žunić, T., and Surour, A.A. (2010) Crystal structure analysis of four tourmalines from the Cleopatra's Mines (Egypt) and Jabal Zalm (Saudi Arabia), and the role of Al in the tourmaline group. American Mineralogist, 95, 510–518.

Burns, P.C., MacDonald, D.J., and Hawthorne, F.C. (1994) The crystal chemistry of manganese-bearing elbaite. Canadian Mineralogist, 32, 31–41.

Clark, C.M., Hawthorne, F.C, and Ottolini, L. (2011) Fluor-dravite, $NaMg_3Al_6Si_6O_{18}(BO_3)_3(OH)_3F$, a new mineral of the tourmaline group from the Crabtree emerald mine, Mitchell county, North Carolina: Description and crystal structure. Canadian Mineralogist, 49, 57–62.

Dutrow, B.L., and Henry, D.J. (2011) Tourmaline: A geologic DVD. Elements, 7, 301–306.

Ertl, A., Rossman, G.R., Hughes, J.M., London, D., Wang, Y., O'Leary, J.A., Dyar. M.D., Prowatke, S., Ludwig, T., and Tillmanns, E. (2010a) Tourmaline of the elbaite-schorl series from the Himalaya Mine, Mesa Grande, California: A detailed investigation. American Mineralogist, 95, 24–40.

Ertl, A., Marschall, H.R., Giester, G., Henry, D.J., Schertl, H.P., Ntaflos, T., Luvizotto, G.L., Nasdala, L., and Tillmanns, E. (2010b) Metamorphic ultrahigh-pressure tourmaline: Structure, chemistry, and correlations to P-T conditions. American Mineralogist, 95, 1–10.

Grice, J.D., Ercit, T.S., and Hawthorne, F.C. (1993) Povondraite, a redefinition of the tourmaline ferridravite. American Mineralogist, 78, 433–436.

Hawthorne, F.C. (1996) Structural mechanisms for light-element variations in tourmaline.

313 Canadian Mineralogist, 34, 123–132.
314 ——— (2002) Bond-valence constraints on the chemical composition of tourmaline. Canadian
315 Mineralogist, 40, 789–797.
316 Hawthorne, F.C., and Dirlam, D.M. (2011) Tourmaline, the indicator mineral: From atomic
317 arrangement to Viking navigation. Elements, 7, 307–312.
318 Hawthorne, F.C., and Henry, D.J. (1999) Classification of the minerals of the tourmaline group.
319 European Journal of Mineralogy, 11, 201–215.
320 Hawthorne, F.C., MacDonald, D.J., and Burns, P.C. (1993) Reassignment of cation site-
321 occupancies in tourmaline: Al/Mg disorder in the crystal structure of dravite. American
322 Mineralogist, 78, 265–270.
323 Hawthorne, F.C, Ungaretti, L., and Oberti, R. (1995) Site populations in minerals: terminology
324 and presentation of results of crystal-structure refinement. Canadian Mineralogist, 33,
325 907–911.
326 Henry, D.J., and Dutrow, B.L. (1990) Ca substitution in Li-poor aluminous tourmaline. Canadian
327 Mineralogist, 28, 111–124.
328 Henry, D.J., and Dutrow, B.L. (1996) Metamorphic tourmaline and its petrologic applications.
329 Reviews in Mineralogy, 33, 503–557.
330 Henry, D.J., and Dutrow, B.L. (2011) The incorporation of fluorine in tourmaline: Internal
331 crystallographic controls or external environmental influences? Canadian Mineralogist,
332 49, 41–56.
333 Henry, D.J., Novák, M., Hawthorne, F.C., Ertl, A., Dutrow, B.L., Uher, P., and Pezzotta, F.
334 (2011) Nomenclature of the tourmaline super-group minerals. American Mineralogist,
335 96, 895–913.

Hezel, D.C., Kalt, A., Marschall, H.R., Ludwig, T., and Meyer, H.-P. (2011) Major-element and Li, Be compositional evolution of tourmaline in an S-type granite–pegmatite system and its country rocks: an example from Ikaria, Aegean Sea, Greece. Canadian Mineralogist, 49, 321–340.

Hwang, S.L., Shen, P., Chu, H.T., Yui, T.F., Liou, J.G., Sobolev, N.V., and Shatsky, V.S. (2005) Crust-derived potassic fluid in metamorphic microdiamond. Earth and Planetary Science Letters, 231, 295–306.

Kaneko, Y., Maruyama, S., Terabayashi, M., Yamamoto, H., Ishikawa, M., Anma, R., Parkinson, C.D., Ota, T., Nakajima, Y., Katayama, I., Yamamoto, J., and Yamauchi, K. (2000) Geology of the Kokchetav UHP-HP metamorphic belt, Northern Kazakhstan. The Island Arc, 9, 264–283.

Ludwig, T., Marschall, H.R., Pogge von Strandmann, P.A.E., Shabaga, B.M., Fayek, M., and Hawthorne, F.C. (2011) A secondary ion mass spectrometry (SIMS) re-evaluation of B and Li isotopic compositions of Cu-bearing elbaite from three global localities. Mineralogical Magazine, 75, 2485–2494.

Lussier, A.J., and Hawthorne, F.C. (2011) Oscillatory zoned liddicoatite from central Madagascar. II. Compositional variations and substitution mechanisms. Canadian Mineralogist, 49, 89–104.

Lussier, A.J., Aguiar, P.M., Michaelis, V.K., Kroeker, S., Herwig, S., Abdu, Y., and Hawthorne, F.C. (2008) Mushroom elbaite from the Kat Chay mine, Momeik, near Mogok, Myanmar: I. Crystal chemistry by SREF, EMPA, MAS NMR and Mössbauer spectroscopy. Mineralogical Magazine, 72, 747–761.

Lussier, A.J., Hawthorne, F.C., Aguiar, P.M., Michaelis, V.K., and Kroeker, S. (2011a) Elbaite-

liddicoatite from Black Rapids glacier, Alaska. Periodico di Mineralogia, 80, 57–73.

Lussier, A.J., Abdu, Y. Hawthorne, F.C., Michaelis, V.K., Aguiar, P.M., and Kroeker, S. (2011b) Oscillatory zoned liddicoatite from Anjanabonoina, central Madagascar. I. Crystal chemistry and structure by SREF and 11B and 27Al MAS NMR spectroscopy. Canadian Mineralogist, 49, 63–88.

MacDonald, D.J., and Hawthorne, F.C. (1995) The crystal chemistry of Si ↔ Al substitution in tourmaline. Canadian Mineralogist, 33, 849–858.

MacDonald, D.J., Hawthorne, F.C., and Grice, J.D. (1993) Foitite, $\square[Fe^{2+}_2(Al,Fe^{3+})]Al_6Si_6O_{18}(BO_3)_3(OH)_4$, a new alkali-deficient tourmaline: description and crystal structure. American Mineralogist, 78, 1299–1303.

Marschall, H.R., and Jiang, S.-Y. (2011) Tourmaline Isotopes: No element left behind. Elements, 7, 313–319.

Marschall, H.R., Ludwig, T., Altherr, R., Kalt, A., and Tonarini, S. (2006) Syros metasomatic tourmaline: Evidence for very high-δ11B fluids in subduction zones. Journal of Petrology, 47, 1915–1942.

McKeown, D.A. (2008) Raman spectroscopy, vibrational analysis and heating of buergerite tourmaline. Physics and Chemistry of Minerals, 35, 259–270.

Novák, M., Povondra, P., and Selway, J.B. (2004) Schorl-oxy-schorl to dravite-oxy-dravite tourmaline from granitic pegmatites; examples from the Moldanubicum, Czech Republic. European Journal of Mineralogy, 16, 323–333.

Novák, M., Škoda, P., Filip, J., Macek, I., and Vaculovič, T. (2011) Compositional trends in tourmaline from intragranitic NYF pegmatites of the Třebíč Pluton, Czech Republic; electron microprobe, Mössbauer and LA-ICP-MS study. Canadian Mineralogist, 49, 359–

380.

Novák, M., Ertl, A., Povondra, P., Galiová, M.V., Rossman, G.R., Pristacz, H., Prem, M., Giester, G., Gadas, P., and Škoda, R. (2013) Darrellhenryite, $Na(LiAl_2)Al_6(BO_3)_3Si_6O_{18}(OH)_3O$, a new mineral from the tourmaline supergroup. American Mineralogist, 98, 1886–1892.

Ogasawara, Y., Fukasawa, K., and Maruyama, S. (2002) Coesite exsolution from supersilicic titanite in UHP marble from the Kokchetav Massif, northern Kazakhstan. American Mineralogist, 87, 454–461.

Ota, T., Kobayashi, K., Katsura, T., and Nakamura, E. (2008a) Tourmaline breakdown in a pelitic system: implications for boron cycling through subduction zones. Contributions to Mineralogy and Petrology, 155, 19–32.

——— (2008b) Boron cycling by subducted lithosphere; insights from diamondiferous tourmaline from the Kokchetav ultrahigh-pressure metamorphic belt. Geochimica et Cosmochimica Acta, 72, 3531–3541.

Pertlik, F., Ertl, A., Körner, W., Brandstätter, F., and Schuster, R. (2003) Na-rich dravite in the marbles from Friesach, Carinthia, Austria: Chemistry and crystal structure. Neues Jahrbuch für Mineralogie Monatshefte, 2003, 277-288.

Pouchou, J.L., and Pichoir, F. (1985) 'PAP' φ(ρZ) procedure for improved quantitative microanalysis. In J.T. Armstrong, Ed., Microbeam Analysis, p. 104–106. San Francisco Press, San Francisco, California.

Rancourt D.G., and Ping J.Y. (1991) Voigt-based methods for arbitrary-shape static hyperfine parameter distributions in Mössbauer spectroscopy. Nuclear Instruments and Methods in Physics Research, B58, 85–97.

Selway, J.B., Černý, P., and Hawthorne, F.C. (1998a) Feruvite from lepidolite pegmatites at Red Cross lake, Manitoba. Canadian Mineralogist, 36, 433–439.

Selway, J.B., Novák, M., Hawthorne, F.C., Černý, P., Ottolini, L., and Kyser, T.K. (1998b) Rossmanite, $\square[LiAl_2]Al_6Si_6O_{18}(BO_3)_3(OH)$, a new alkali-deficient tourmaline: Description and crystal structure. American Mineralogist, 83, 896–900.

Selway, J.B., Novák, M. Černý, P., and Hawthorne, F.C. (1999) Compositional evolution of tourmaline in lepidolite-subtype pegmatites. European Journal of Mineralogy, 11, 569–584.

Selway, J.B., Černý, P., Hawthorne, F.C., and Novák, M. (2000a) The Tanco pegmatite at Bernic Lake, Manitoba. XIV. Internal tourmaline. Canadian Mineralogist, 38, 877–891.

Selway, J.B., Novák, M., Černý, P., and Hawthorne, F.C. (2000b) The Tanco pegmatite at Bernic Lake, Manitoba. XIII. Exocontact tourmaline. Canadian Mineralogist, 38, 869–976.

Selway, J.B., Smeds, S-A., Černý, P., and Hawthorne, F.C. (2002) Compositional evolution of tourmaline in the petalite-subtype Nyköpingsgruvan pegmatites, Utö, Stockholm Archipelago, Sweden. GFF, 124, 93–102.

Shabaga, B.M., Fayek, M., and Hawthorne, F.C. (2010) Boron and lithium isotopic compositions as provenance indicators of Cu-bearing tourmalines. Mineralogical Magazine, 74, 241–255.

Sheldrick, G.M. (2008) A short History of SHELX. Acta Crystallographica, A64, 112–122.

Shimizu, R., and Ogasawara, Y. (2013) Diversity of potassium-bearing tourmalines in diamondiferous Kokchetav UHP metamorphic rocks: a geochemical recorder from peak to retrograde metamorphic stages. Journal of Asian Earth Science, 63, 39–55.

Skogby, H., Bosi, F., and Lazor, P. (2012) Short-range order in tourmaline: a vibrational

spectroscopic approach to elbaite. Physics and Chemistry of Minerals, 39, 811–816.

Taylor, M.C., Cooper, M.A., and Hawthorne, F.C. (1995) Local charge-compensation in hydroxyl-deficient uvite. Canadian Mineralogist, 33, 1215–1221.

van Hinsberg, V.J., and Marschall, H.R. (2007) Boron isotope and light element sector zoning in tourmaline: Implications for the formation of B-isotopic signatures. Chemical Geology, 238, 141–148.

van Hinsberg, V.J., and Schumacher, J.C. (2009) The geothermobarometric potential of tourmaline, based on experimental and natural data. American Mineralogist, 94, 761–770.

van Hinsberg, V.J., Henry, D.J., and Dutrow, B.L. (2011a) Tourmaline as a petrologic forensic mineral: A unique recorder of its geologic past. Elements, 7, 327–332.

van Hinsberg, V.J., Henry, D.J., and Marschall, H.R. (2011b) Tourmaline: an ideal indicator of its host environment. Canadian Mineralogist, 49, 1–16.

Wunder, B., Berryman, E., Plessen, B., Rhede, D., Koch-Muller, M., and Heinrich, W. (2015) Synthetic and natural ammonium-bearing tourmaline. American Mineralogist, 100, 250–256.

Zácek, V., Jirá, F., Petrov, A., and Hyrsl, J. (2000) Tourmalines of the povondraite-(oxy) dravite series from the cap rock of meta-evaporite in Alto Chapare, Cochabamba, Bolivia. Journal of the Czech Geological Society, 45, 3–12.

# FIGURE CAPTIONS

**Figure 1.** (A) Photomicrograph and (B) characteristic X-ray K-*K*α map of diamondiferous K-bearing tourmaline. Tourmaline shows discontinuous chemical zoning with representative K-contents in apfu of 0.58 (core), 0.15 (mantle), and 0.04 (rim). Diamond inclusions occur only in the K-dominant tourmaline core, i.e., maruyamaite (shown bounded by red broken lines). Abbreviations in (A) are: Dia: diamond, Gr: graphite, Kfs: K-feldspar, Qz: quartz, and Tur: tourmaline.

**Figure 2.** Raman spectra of maruyamaite with the laser (a) perpendicular, and (b) parallel to the *c*-axis.

**Figure 3.** Mössbauer spectrum of maruyamaite; Full lines: $Fe^{2+}$ doublets, dashed line: $Fe^{3+}$ doublet.

**Figure 4.** Variation in <*Z*-O> as a function of the $^{Z}$Al* (= Al + $Fe^{3+}$) content at the Z site for selected tourmalines; uvites from McDonald and Hawthorne (1995) (green circles) and Clark et al. (unpublished) (yellow circle); dravites from Bosi and Lucchesi (2004) (samples 235a, 235b, 65e, red circles) and Pertlik et al. (2003) (blue circle). The dashed line shows extrapolation of holotype maruyamaite (pink diamond) to the regression line defined by the rest of the data and the corresponding value of $^{Z}$Al indicated by the dashed arrow: 5.00 apfu.

**TABLE 1.** Mössbauer parameters (mm/s) for maruyamaite

| Cation | Centre shift (mm/s) | Quadrupole splitting | Area ratio |
|---|---|---|---|
| $Fe^{2+}$ | 1.086(8) | 2.46(15) | 44(5) |
| $Fe^{2+}$ | 1.099(20) | 1.89(5) | 49(5) |
| $Fe^{3+}$ | 0.35(10) | 0.66(28) | 2(1.8) |

**TABLE 2.** Chemical composition (wt%) for maruyamaite

| Constituent | Wt% | Range | Standard deviation |
|---|---|---|---|
| $SiO_2$ | 36.37 | 35.83–36.74 | 0.30 |
| $TiO_2$ | 1.09 | 0.90–1.21 | 0.03 |
| $Al_2O_3$ | 31.50 | 31.25–32.06 | 0.11 |
| $B_2O_3$ | 10.58 | – | – |
| $Cr_2O_3$ | 0.04 | 0.01–0.06 | 0.01 |
| FeO* | 4.28 | 4.07–4.55 | 0.02 |
| $Fe_2O_3$ | 0.33 | – | – |
| FeO | 4.01 | – | – |
| MgO | 9.00 | 8.78–9.19 | 0.10 |
| CaO | 1.47 | 1.39–1.55 | 0.01 |
| $Na_2O$ | 0.60 | 0.52–0.65 | 0.03 |
| $K_2O$ | 2.54 | 2.43–2.64 | 0.05 |
| F | 0.30 | 0.20–0.37 | 0.05 |
| $H_2O$ | 2.96 | – | – |
| O = F | -0.13 | – | – |
| Total | 100.67 | – | – |

* FeO determined by electron-microprobe analysis.

**TABLE 3.** Powder-diffraction pattern for maruyamaite

| $I_{rel}$ | $d_{(meas.)}$ Å | $d_{(calc.)}$ Å | $h$ | $k$ | $l$ | $I_{rel}$ | $d_{(meas.)}$ Å | $d_{(calc.)}$ Å | $h$ | $k$ | $l$ |
|---|---|---|---|---|---|---|---|---|---|---|---|
| **23** | **6.415** | **6.404** | **-1** | **1** | **1** | 15 B | 2.132* | 2.135 | -3 | 3 | 3 |
| 21 | 5.002 | 4.994 | 0 | 2 | 1 | | | 2.135 | 0 | 3 | 3 |
| 20 | 4.610 | 4.605 | 0 | 3 | 0 | **54** | **2.046** | **2.046** | **-1** | **6** | **2** |
| **59** | **4.237** | **4.233** | **-2** | **3** | **1** | 7 | 1.994 | 1.994 | -4 | 8 | 0 |
| **69** | **3.995** | **3.988** | **-2** | **4** | **0** | **36** | **1.923** | **1.923** | **-3** | **7** | **2** |
| **42** | **3.498** | **3.496** | **0** | **1** | **2** | 6 | 1.883 | 1.882 | -1 | 5 | 3 |
| 12 | 3.389 | 3.386 | -1 | 4 | 1 | 10 | 1.852 | 1.852 | -6 | 8 | 1 |
| 2 | 3.204 | 3.202 | -2 | 2 | 2 | 2 B | 1.825* | 1.820 | -6 | 7 | 2 |
| 3 | 3.113 | 3.116 | -4 | 4 | 1 | 6 B | 1.787* | 1.792 | -1 | 1 | 4 |
| **85** | **2.974** | **2.972** | **-1** | **3** | **2** | | | 1.785 | -3 | 6 | 3 |
| 12 | 2.904 | 2.903 | -3 | 5 | 1 | 3 B | 1.746 | 1.748 | 0 | 2 | 4 |
| 10 | 2.634 | 2.629 | -3 | 4 | 2 | 5 | 1.692 | 1.693 | -2 | 8 | 2 |
| **100** | **2.581** | **2.581** | **0** | **5** | **1** | 21 | 1.664 | 1.665 | -6 | 6 | 3 |
| 2 | 2.495 | 2.497 | 0 | 4 | 2 | | | 1.665 | 0 | 6 | 3 |
| 3 | 2.456 | 2.456 | -2 | 6 | 1 | 18 | 1.644 | 1.644 | -2 | 9 | 1 |
| 14 B | 2.386* | 2.409 | 0 | 0 | 3 | 22 | 1.595 | 1.595 | -5 | 10 | 0 |
| | | 2.383 | -2 | 5 | 2 | 5 | 1.547 | 1.548 | 4 | -10 | 1 |
| 19 | 2.347 | 2.347 | -5 | 6 | 1 | 11 | 1.530* | 1.535 | 0 | 9 | 0 |
| 4 B | 2.305* | 2.306 | -1 | 2 | 3 | | | 1.529 | -7 | 9 | 2 |
| | | 2.303 | 0 | 6 | 0 | 19 | 1.511 | 1.512 | 0 | 5 | 4 |
| 11 | 2.196 | 2.195 | -5 | 5 | 2 | 4 | 1.485 | 1.486 | -2 | 6 | 4 |
| 18 | 2.168 | 2.167 | -4 | 7 | 1 | 15 | 1.458* | 1.461 | -5 | 6 | 4 |

{note to typesetting: minus signs are overbars in above table}

**TABLE 4.** Miscellaneous information for maruyamaite

| | | | |
|---|---|---|---|
| *a* (Å) | 15.955(10) | crystal size (μm) | 30 x 60 x 80 |
| *c* | 7.227(4) | radiation | Mo*K*α |
| *V* (Å$^3$) | 1593(2) | No. unique reflections | 1149 |
| | | No. $\|F_o\| > 5\sigma F$ | 1149 |
| Space group | *R*3*m* | $R_{int}$ % | 1.02 |
| Z | 3 | $R_{obs}$ % | 1.58 |
| $D_{calc.}$ (gcm$^{-3}$) | 3.081 | $wR_2$ % | 3.98 |
| | | GOF | 1.131 |

**TABLE 5.** Atom coordinates and displacement parameters for maruyamaite

| Atom | *x* | *y* | *z* | $U_{11}$ | $U_{22}$ | $U_{33}$ | $U_{23}$ | $U_{13}$ | $U_{12}$ | $U_{eq}$ |
|---|---|---|---|---|---|---|---|---|---|---|
| *X* | 0 | 0 | 0.2206(2) | 0.0154(6) | 0.0154(6) | 0.0227(8) | 0 | 0 | 0.0077(3) | 0.0178(5) |
| *Y* | 0.12420(5) | 0.06210(3) | 0.63605(12) | 0.0105(4) | 0.0079(3) | 0.0176(4) | –0.00237(12) | –0.0048(2) | 0.00526(19) | 0.0117(2) |
| *Z* | 0.29818(4) | 0.26169(4) | 0.61244(11) | 0.0068(2) | 0.0066(3) | 0.0071(2) | 0.00016(18) | –0.00038(18) | 0.00330(19) | 0.00684(13) |
| *T* | 0.19192(3) | 0.19010(3) | 1.00 | 0.0055(2) | 0.0055(2) | 0.0077(2) | –0.00091(16) | –0.00071(17) | 0.00256(16) | 0.00633(12) |
| *B* | 0.10985(11) | 0.2197(2) | 0.4561(4) | 0.0078(8) | 0.0079(12) | 0.0082(11) | 0.0006(9) | 0.0003(4) | 0.0040(6) | 0.0079(5) |
| O1 | 0 | 0 | 0.7753(5) | 0.0151(10) | 0.0151(10) | 0.0106(15) | 0 | 0 | 0.0075(5) | 0.0136(7) |
| O2 | 0.06089(8) | 0.12178(15) | 0.4875(3) | 0.0138(7) | 0.0075(9) | 0.0175(10) | 0.0014(7) | 0.0007(3) | 0.0037(5) | 0.0136(4) |
| O3 | 0.26395(18) | 0.13197(9) | 0.5127(3) | 0.0282(12) | 0.0148(7) | 0.0069(8) | –0.0000(4) | –0.0000(8) | 0.0141(6) | 0.0151(4) |
| O4 | 0.09278(8) | 0.18556(15) | 0.0708(3) | 0.0083(6) | 0.0145(10) | 0.0114(8) | –0.0016(7) | –0.0008(4) | 0.0073(5) | 0.0107(4) |
| O5 | 0.18438(16) | 0.09219(8) | 0.0920(3) | 0.0153(10) | 0.0077(6) | 0.0119(8) | 0.0002(3) | 0.0003(7) | 0.0077(5) | 0.0108(4) |
| O6 | 0.19555(10) | 0.18571(10) | 0.7784(2) | 0.0114(6) | 0.0112(6) | 0.0073(6) | –0.0013(5) | –0.0008(5) | 0.0062(5) | 0.0098(3) |
| O7 | 0.28470(10) | 0.28492(9) | 0.07961(19) | 0.0073(6) | 0.0069(6) | 0.0104(6) | –0.0014(5) | –0.0015(5) | 0.0014(5) | 0.0091(3) |
| O8 | 0.20934(10) | 0.26999(11) | 0.4420(2) | 0.0056(6) | 0.0101(6) | 0.0161(6) | 0.0022(5) | 0.0005(5) | 0.0039(5) | 0.0106(3) |

**TABLE 6.** Selected interatomic distances (Å) in maruyamaite

| | | | | | |
|---|---|---|---|---|---|
| *X*-O2 | | 2.560(2) | *Z*-O3 | | 1.993(1) |
| *X*-O4 | | 2.783(2) | *Z*-O6 | | 1.898(1) |
| *X*-O5 | | 2.712(2) | *Z*-O7 | | 1.907(1) |
| <*X*-O> | | 2.685 | *Z*-O7 | | 1.963(1) |
| | | | *Z*-O8 | | 1.900(1) |
| *T*-O4 | | 1.629(1) | *Z*-O8 | | 1.932(1) |
| *T*-O5 | | 1.646(1) | <*Z*-O> | | 1.932 |
| *T*-O6 | | 1.606(1) | | | |
| *T*-O7 | | 1.604(1) | *Y*-O1 | | 1.990(2) |
| <*T*-O> | | 1.621 | *Y*-O2 | x2 | 2.011(1) |
| | | | *Y*-O3 | | 2.127(2) |
| *B*-O2 | | 1.372(3) | *Y*-O6 | x2 | 1.999(1) |
| *B*-O8 | x2 | 1.379(2) | <*Y*-O> | | 2.023 |
| <*B*-O> | | 1.377 | | | |

**TABLE 7.** Site-scattering values (*epfu*) and assigned site occupancies in maruyamaite

| Site | Site population (*apfu*) from EMPA | Site scattering (*epfu*) | |
|---|---|---|---|
| | | refined | calculated |
| *X* | 0.53 K + 0.19 Na + 0.26 Ca | 16.6(1) | 17.3 |
| *Y* | 1.19 Mg + 0.55 $Fe^{2+}$ + 0.05 $Fe^{3+}$ + 1.07 Al + 0.14 Ti | 46.9(6) | 46.4 |
| *Z* | 5.00 Al + 1.00 Mg | 78* | 77 |
| *T* | 5.97 Si + 0.03 Al | 84* | 84 |

* fixed.

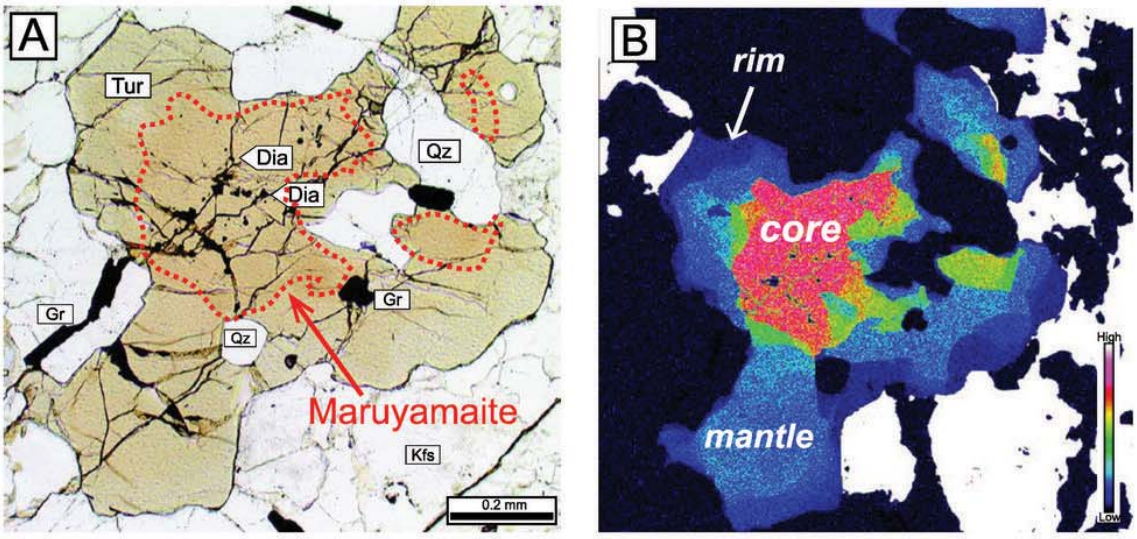
A
Tur
Dia
Dia
Qz
Gr
Gr
Qz
Maruyamaite
Kfs
0.2 mm
B
rim
core
mantle
High
Low

FIGURE 1

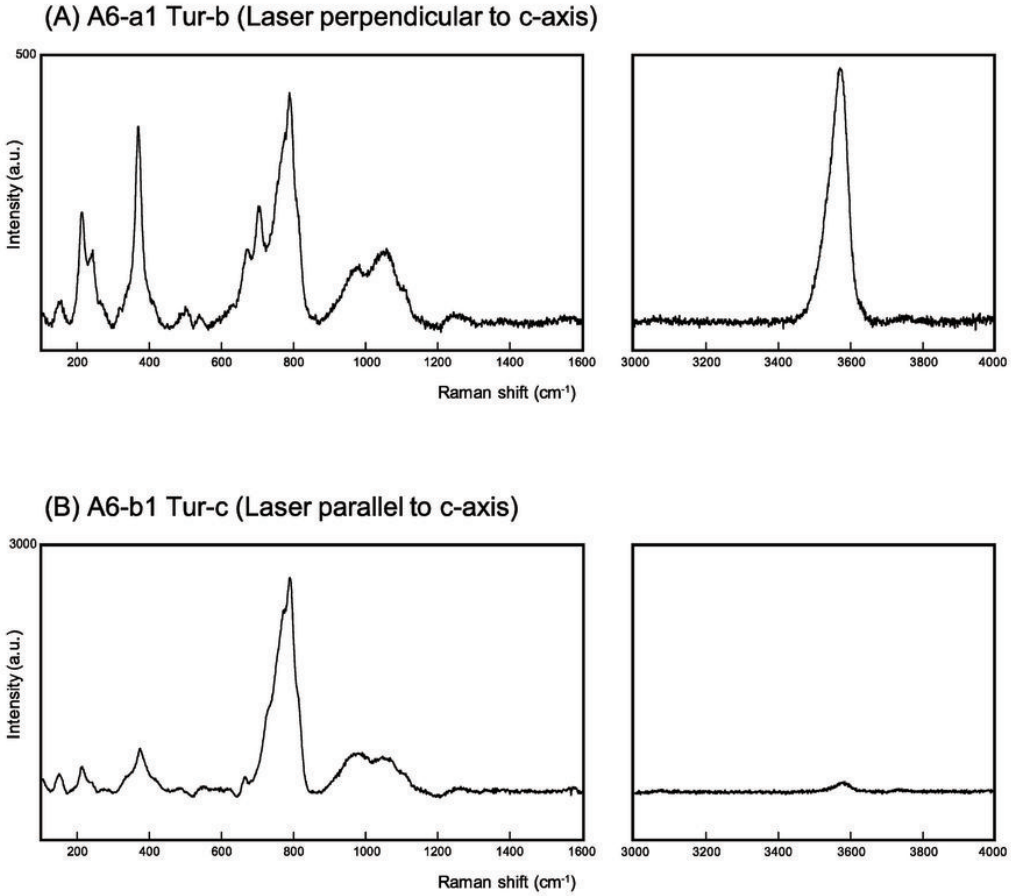
(A) A6-a1 Tur-b (Laser perpendicular to c-axis)
Intensity (a.u.)
Raman shift (cm-1)
(B) A6-b1 Tur-c (Laser parallel to c-axis)
Intensity (a.u.)
Raman shift (cm-1)

FIGURE 2

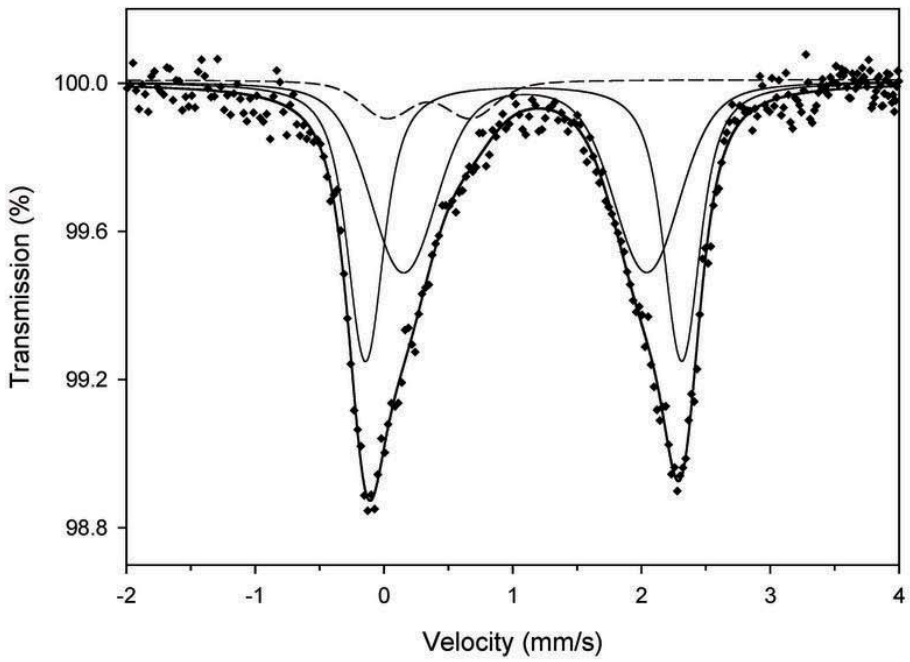


FIGURE 3

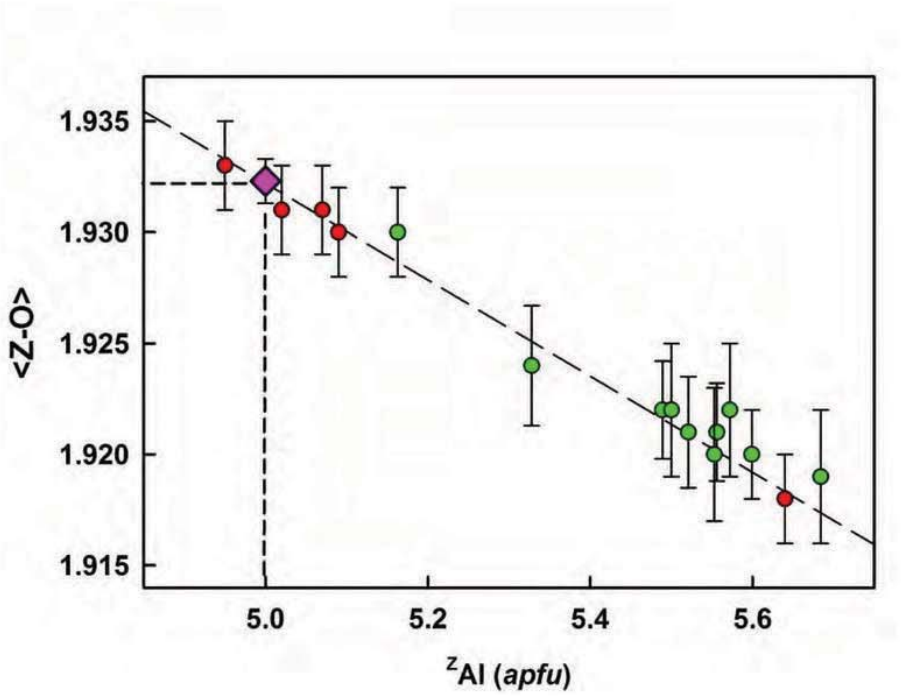


FIGURE 4